All-Fiber All-Optical Quantitative Polymerase Chain Reaction (qPCR)

Xuegang Li[a,b,*], Linh V. Nguyen[b], Kelly Hill[c,d], Heike Ebendorff-Heidepriem[b,e], Erik P. Schartner[b,e], Yong Zhao[a], Xue Zhou[a], Yanan Zhang[a], and Stephen C. Warren-Smith[b,e]

[a]*College of Information Science and Engineering, Northeastern University, Shenyang, Liaoning 110819, China*
[b]*Institute for Photonics and Advanced Sensing and School of Physical Sciences, The University of Adelaide, Adelaide, SA 5005, Australia*
[c]*South Australian Research and Development Institute, Urrbrae, SA 5064, Australia*
[d]*School of Agriculture, Food and Wine, The University of Adelaide, Adelaide, SA 5005, Australia*
[e]*ARC Centre of Excellence for Nanoscale BioPhotonics, The University of Adelaide, Adelaide, SA 5005, Australia*

**corresponding author: lixuegang@ise.neu.edu.cn, +86 15840383617*

Abstract: Quantitative polymerase chain reaction (qPCR), the real-time amplification and measurement of a targeted DNA molecule, has revolutionized the biological sciences and is routinely applied in areas such as medical diagnostics, forensics, and agriculture. Despite enormous potential in biological research and medicine, the availability of low-cost and high-speed field-portable systems remains to be a significant barrier to widescale implementation. Here we propose and demonstrate a potential solution using a photonics-based qPCR system. By using an all-optical approach, we achieve ultra-fast temperature response with real-time temperature feedback using nanoliter scale reaction volumes. The system uses a microcavity to act as a nanoliter scale reaction vessel with a laser-driven and optically monitored temperature cycling system for ultrafast thermal cycling and incorporates an all-fiber fluorescence excitation/detection system to achieve real-time, high sensitivity fluorescence monitoring of the qPCR process. Further, we demonstrate the potential of the system to operate as a label-free qPCR system through direct optical measurement of the sample refractive index. Due to advantages in portability and fabrication simplicity, we anticipate that this platform technology will offer a new strategy for fundamental techniques in biochemistry applications, such as point-of-care and remote diagnostics.

Keywords: Quantitative polymerase chain reaction; Optical fiber device; Optical fiber sensing; Microfluidics; Microcavity, Label-free.

1. Introduction

The polymerase chain reaction (PCR) technique was invented by Kary Mullis in 1984 [1,2], which has since been used to amplify individual deoxyribonucleic acid (DNA) segments for sequencing, genotyping and cloning. PCR technology is now one of the most important tools in biochemistry [3-7]. End-point PCR using traditional visualization methods, such as gel-

electrophoresis, has evolved over the years in terms of reaction components, primer numbers and targets, and detection systems. These changes have been utilized to increase specificity, sensitivity, quantification, speed and to allow for automation.

Quantitative polymerase chain reaction (qPCR) is a technique that combines amplification and detection into a single process. Examples of qPCR applications include forensics [8], cancer diagnostics [9], Alzheimer's detection [10], stem cell research [11], and single-cell profiling [12,13]. The related quantitative reverse-transcription PCR (qRT-PCR) technique, for the detection of ribonucleic acid (RNA), utilizes the same underlying principle following reverse transcription of RNA into DNA and is the basis for testing many important viruses including influenza [14]and SARS-CoV-2[15,16]. The qPCR platform integrates two steps: temperature cycling and detection, where detection is typically via fluorescence. Detection relies on one of two mechanisms: fluorescent dye integration into amplified double stranded products; or degradation of a dual labelled probe which resides between two external primers. Here we use the latter approach whereby a quenched fluorophore (from intact probe oligonucleotide), is released during thermal cycling and the measured fluorescence signal is proportional to the amplified DNA. Of particular interest is the fluorescence signal during the exponential phase of the reaction, which yields information on the initial quantity of the DNA template, hence the name "quantitative PCR."

While commercial qPCR systems are widely adopted in laboratory settings, developing portable, reliable and low-cost point-of-care devices is an area of active research. It is widely acknowledged, such as by the Bill and Melinda Gates Foundation, that such devices would particularly benefit healthcare in the developing world [17]. However, Petralia and Conoci note that despite the maturity of PCR chemistry and technologies, there are very few commercial point-of-care devices available [7]. This is due to the requirement that qPCR systems incorporate multiple elements, including micro-fluidics, a thermal cycling element, a temperature sensor, and a detection (namely fluorescence) unit. A particular limiting factor is the thermal cycling, with standard conduction-based methods typically having slow heating and cooling rates, meaning the qPCR thermal cycling stage can take 45–180 minutes [18]. While alternative techniques for isothermal PCR are being actively developed, such as loop-mediated isothermal amplification, thermal-based qPCR is still more sensitive and remains the gold standard for quantitative detection of targets in mixed samples [19]. Thus, under comparable PCR reaction conditions (number of thermal cycles, denaturation/anneal/extend temperatures), improving the thermal cycling efficiency is the preferred way to decrease assay times.

There have been numerous designs proposed to improve the thermal cycling efficiency. One approach is the use of microfluidic chips, where micro-droplets are loaded and actuated through the chip via methods such as vacuum pumping [20], electro wetting actuation [21], the use of a magnet on magnetic bead filled droplets [22], and capillary action [23]. A powerful benefit of this technique is that the qPCR mix can be moved between zones of different temperatures for the denaturation, annealing and extension steps [24]. However, the challenge with this approach is the precise control of the thermal and fluidic properties of the relatively small microfluidic chip [18], particularly if it is to be used as a point-of-care device with varying environmental conditions.

An alternative approach is to reduce the reaction volume to the nanoliter scale, enabling faster thermal transfer and thus reducing the thermal cycling duration. This is common with digital PCR, where the sample is split into many (order of hundreds to millions) partitions that contain either zero or one template DNA, which are subsequently counted to provide a digital readout of the original DNA template quantity [25,26]. While portable digital PCR systems are under development, such as via integration with smartphone technology [27], the limitation of the currently available digital PCR systems is the high cost.

The concept of using micro/nano-droplets can, of course, be used in a traditional qPCR configuration to offer high speed thermal cycling. Recent demonstrations have shown that optically pumped systems offer particularly fast and controllable thermal cycling performance. This can be achieved through plasmonically mediated heating with gold films [28] and gold nanoparticles [29], or more directly by targeting the near-infrared (≈1.45 μm) absorption peak of water [30,31]. In this case dozens of PCR cycling steps can be achieved in the order of minutes or less. However, these demonstrations have been achieved using bulky setups, such as requiring a fluorescence microscope [30,31]. Indeed, the requirement for fluorescence detection in itself limits the potential portability of the system given the requirements for filters, light source, detector and sample positioning for measurement.

Optical fibers offer several advantages for field-portable and low-power qPCR given their inherent multiplexing capability, small size, and the vast array of portable fiber-integrated components that have arisen due to the telecommunications industry. This has already been proven in fields ranging from large scale structural health monitoring [32,33] through to biomedical applications [34-39]. Several optical fiber sensing schemes have been demonstrated for the detection of single-stranded DNA (ssDNA). For example, complementary ssDNA can be immobilized onto an optical fiber such as for the detection of quantum dot labelled ssDNA [40] or label-free detection using gold coated tapers fibers [41]. In our previous work, we demonstrated DNA detection with nanoliter samples by immobilizing molecular beacons to the internal

surface of microstructured optical fiber [42-44]. However, these techniques are limited to relatively large concentrations of DNA and misses out on the amplification power of qPCR that allows it to detect and quantify ultra-low concentrations of DNA.

In this paper, we demonstrate an all-fiber all-optical qPCR system with ultra-fast temperature response, real-time temperature feedback, and nanoliter scale reaction volume, with strong potential for use as a portable, point-of-care device. The use of fiber optics provides the opportunity to implement a fully integrated system, while taking advantage of the optical fiber's well-known characteristics of being small, lightweight, and cheap. Our system uses a C-fiber microcavity to act as a nanoliter scale reaction container as well as a temperature sensor, a temperature cycling system utilizing a near-infrared laser for the ultrafast heating and cooling of the nanoliter sample in the microcavity, and an all-fiber fluorescence excitation/detection system to realize real-time, high sensitivity monitoring of fluorescence during the qPCR process. Further, by monitoring the optical path length of the C-fiber microcavity though optical interferometry, we demonstrate the potential for label-free real-time quantification.

2. Materials and methods

2.1 Operating principle

In general, a fluorescence qPCR system consists of two main parts, (i) thermal cycling of the PCR mix to facilitate DNA amplification and (ii) measuring fluorescence from the PCR mix to confirm DNA amplification.

A schematic diagram of our all-fiber qPCR system based on the optical fiber microcavity, laser ultra-fast heating system, and an all-fiber fluorescence excitation/detection system is illustrated in Figure 1a and 1b. At the center of the system is a microcavity formed by a C-fiber with cross section shown in Figure 1c.

Shown on the right hand side of Figure 1a, thermal cycling is achieved using light from a 1440 nm laser that targets the water absorption peak and is injected into the microcavity via a 3 dB coupler. Simultaneously, the reflection of a swept wavelength laser (1510-1590 nm) is used to detect temperature changes in the Fabry-Perot cavity formed between the two ends of the MMFs. The temperature of the samples can be derived from the fringe shift of the Fabry-Perot reflection spectrum. This temperature value is then used as feedback to the 1440 nm laser controller to form a specified qPCR temperature cycle.

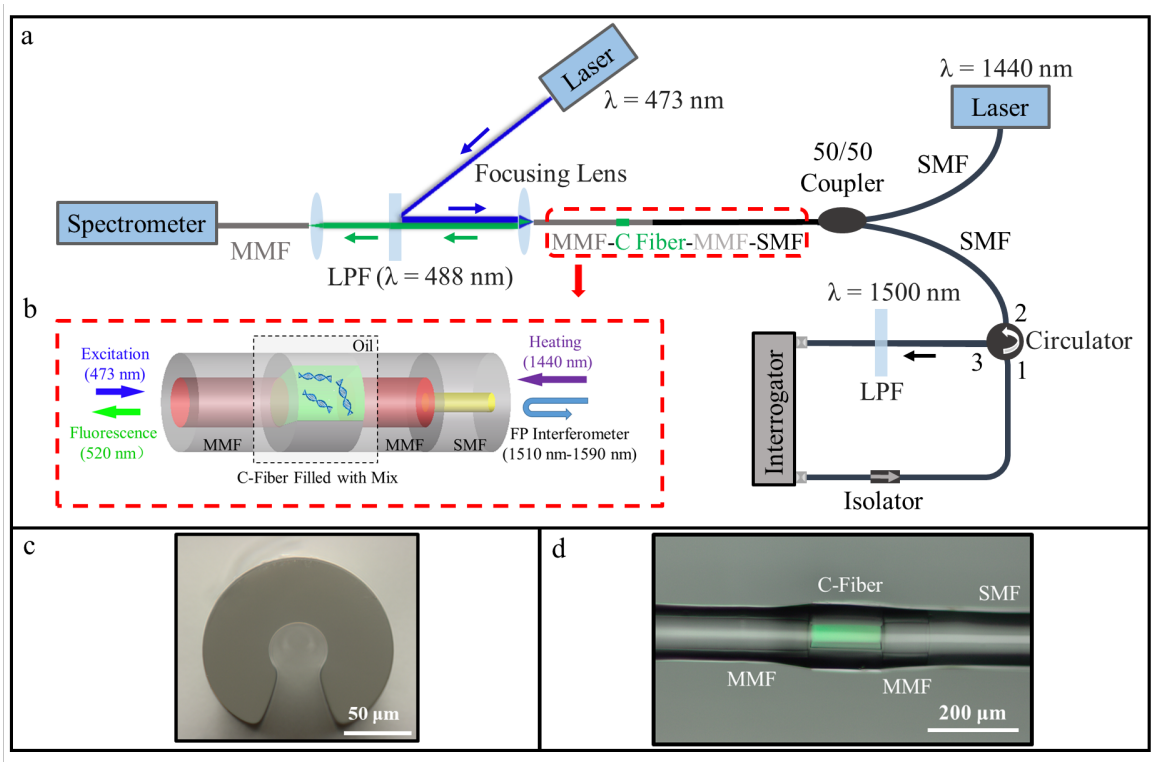

Figure 1. Schematic diagram of the all-fiber qPCR system. (b) Schematic diagram of the C-fiber cavity. (c) Microscope cross sectional image of the C-fiber. (d) Microscope image of the C-fiber cavity filled with 6-Carboxyfluorescein (6-FAM) fluorescent solution. The green inside the C-fiber is the generated fluorescence with the excitation source turned on. Acronyms: LPF, Long Pass Filter; SMF, Single Mode Fiber; MMF, Multimode Fiber.

On the opposite side of the cavity, a fluorescence excitation/detection system based on a 473 nm laser and spectrometer is used to excite and detect the fluorescence of the samples during the qPCR temperature cycles. Figure 1d shows an image of the C-fiber microcavity filled with a solution of 6-Carboxyfluorescein (6-FAM), which is seen to fluorescence under excitation at 473 nm and confirms that the solution was filled into the cavity. Considering that the diameter of the microcavity was 42 μm and the length was 150 μm, the internal reaction volume was approximately 0.2 nL. The reaction volume can be adjusted according to requirements by increasing/reducing the length or diameter of the C-fiber.

2.2 C-fiber and microcavity fabrication

The C-fiber used to form the microcavity is a silica capillary with one side open to allow for fluid ingress [45]. It was fabricated in-house using a two-step technique, which we have previously used to fabricate exposed core microstructured optical fiber [46-48]. Briefly, a preform was first fabricated by ultrasonic drilling a central hole and the cutting the open slot. The preform was then drawn into fiber with 140 μm diameter.

The microcavity was fabricated by splicing a section of the C-fiber between an MMF (50 μm core diameter / 125 μm cladding diameter, fluorescence detection side) and single mode fiber (SMF28, laser heating and temperature measurement side) using an arc splicer (Fujikura FSM-100P). A 100 μm length of MMF was spliced between the SMF and C-fiber to spread the SMF output and allow uniform heating of the filled microcavity. The length of the microcavity can be adjusted by controlling the length of C-fiber. Typically, the length should not be too short compared to the fiber diameter so that the cavity can be filled amply with the sample. Conversely, beam divergence limits the maximum length that can be used. Thus, in this paper we used a 150 μm microcavity, which was experimentally observed to be a good compromise between these two effects.

2.3 Optical system for infrared laser thermal cycling

The infrared laser ultrafast temperature cycling system (shown in Figure 1a) consisted of a 1440 nm laser (QPhotonics, LLC, QFBGLD-1440-250), a swept wavelength optical sensor interrogator (National Instruments PXIe-4844, 1510-1590 nm, 4 pm resolution), a 1500 nm long pass filter (LPF, Thorlabs, FEL1500), a coupler, and a circulator.

The 1440 nm laser was used for ultrafast heating of the reaction, which targets the absorption peak of water [49]. The laser current was controlled with feedback from the temperature measurement described below to achieve the temperature required for qPCR thermal cycling.

The optical sensor interrogator was used to measure the Fabry-Perot reflection spectrum formed in the microcavity. The 1500 nm LPF was used for preventing the 1440 nm laser, 473 nm laser, and 520 nm fluorescence from entering the optical sensor interrogator, which would otherwise give background noise to the temperature measurement. The reflection spectrum of the Fabry-Perot interferometer can be analyzed using a simple two-path interference model,

$$I_{out} = I_1 + I_2 + 2\sqrt{I_1 I_2}\cos(\frac{4\pi L_C}{\lambda} n) \quad , \tag{1}$$

where I_1 and I_2 are light intensities of the two reflections at the MMF/C-fiber interfaces, λ is the free space wavelength, L_C is the length of the C-fiber microcavity, and n is the internal refractive index of the C-fiber microcavity. The refractive index of the PCR mix inside the cavity changes with temperature. Thus, the refractive index inside the cavity, n, at a temperature, T, can be expressed as,

$$n(T) = n(T_0) + \frac{dn}{dT}(T - T_0) \quad , \tag{2}$$

where $n(T_0)$ is the refractive index of the PCR sample is temperature T_0 and dn/dT is, approximately, the thermo-optic coefficient of water. Thus, the Fabry-Perot interferometer can

achieve the measurement of the temperature of the filled liquid by monitoring the change of the Fabry-Perot interference spectrum.

2.4 qPCR master mix and reaction conditions

The human ACTB gene, commonly used as a housekeeping gene for gene expression studies, was used here as a "proof-of-concept" target template [50]. The sequence of the ACTB gBlock gene is: 5'-TACGTGCGTCACATGCAGTACACAGAGCCTCGCCTTTGCCGATCCGCCGCCCGTCCACACCCGCCGCCAGCTCACCATGGATGATGATATCGCCGCGCTCGTCGTCGACAACGGCTCCGGCATGTGCAAGGCACTAGCTCAGATTCAGTAGACCGCTGTTG-3'. Primers and probes were obtained from IDT as pre-designed PrimeTime™ qPCR Probe assay (Hs.PT.39a.22214847), which consists of a primer pair and 5′ nuclease probe at a ratio of 2:1. The primer and probe sequences are as follows:

Primer 1: 5'-CCT TGC ACA TGC CGG AG-3';

Primer 2: 5'-ACA GAG CCT CGC CTT TG-3';

Probe: 5'-/56-FAM/TC ATC CAT G/Zen/G TGA GCT GGC GG/3IABkFQ/-3'.

The probe was labeled using 6-FAM, which has excitation and emission wavelengths of 492 nm and 517 nm, respectively, and a 3' Iowa Black® quencher, which has an absorption spectrum ranging from 420 to 620 nm.

qPCR reactions were carried out as per manufacturer's instructions using the PrimerTime gene expression master mix (2×) for a 20 µL reaction volume. The reaction includes PrimeTime Gene Expression Master Mix (2×) 10 µL, PrimeTime™ qPCR Assay 1 µL, DNA template and nuclease-free water (bring to 20 µL). Reactions carried out within the optical fiber used mineral oil (DNase, RNase, protease, none detected, Sigma-Aldrich) to cover the surface of the PCR mix cavity to achieve heat insulation and prevent qPCR mix outflow. This qPCR mix filled cavity was then placed into a water bath, which was set at 60°C as a baseline temperature for the qPCR experiments.

Manufacturer's instructions were followed for setting up two-step reactions. Briefly, the qPCR cycling conditions included an initial denaturation of 95°C for 3 min followed by 40 cycles of 95°C (denaturation) for 15 s, and 60°C (anneal and extend) for 45 s. No-template control (NTC) reactions were included and run under the same conditions.

2.5 Optical system for fluorescence detection

The fluorescence excitation/detection system, shown in Figure 1a, consisted of a 473 nm laser, a spectrometer (Horiba iHR 550) and a 488 nm LPF (Semrock). The 473 nm laser and spectrometer were used for exciting and detecting the fluorescence of the reaction, respectively.

The 500 nm LPF was used for preventing the excitation laser light (473 nm) from affecting the detection of the emission fluorescence signal (517 nm).

3. Results and Discussion

3.1 Infrared laser thermal cycling

The qPCR system was first characterized to determine the Fabry-Perot interferometer response to temperature by immersing the sealed cavity into a temperature-controlled water bath. The microcavity was filled first with water and then with the qPCR reaction mix, and the Fabry-Perot reflection spectra were recorded at different ambient temperatures (60-95°C with 5°C steps, recorded using the water bath's in-built temperature reference). Three example spectra are shown in Figure 2a for the case of water filled into the cavity, showing a clear shift in the interference spectrum as the temperature was increased. Previous studies have shown that the C-fiber cavity itself is very sensitive to the change of internal refractive index, but is insensitive to temperature when air-filled [51]. Figure 2b shows the corresponding phase change of the Fabry-Perot interference spectra as a function of temperature, which is due to temperature causing a change in refractive index of the solution filling the cavity. It can be seen from Figure 2b that the phase of the Fabry-Perot spectrum decreases with increasing temperature for both the case of water or qPCR reaction mix filled into the microcavity. The two curves are identical, indicating that the thermo-optic coefficient of the qPCR reaction mix is sufficiently similar to water for the water calibration curve to be used for the qPCR experiments.

Figure 2c shows the phase change of the Fabry-Perot spectra as the 1440 nm laser power is increased when the cavity contains either water or the qPCR reaction mix. The second vertical axis shows the corresponding temperature value, as determined from Figure 2b. This demonstrates that the liquid in the microcavity can be heated by the 1440 nm laser and its temperature can be measured in real time with good repeatability and minimal hysteresis. We note that there is a small difference in the heating response of the water and qPCR mix, which we attribute to differences in the absorption coefficient at 1440 nm. Previous studies have shown that different salt solutions will have different absorption coefficients for a given wavelength [52]. Therefore, for the qPCR thermal cycling we used the laser intensity-temperature coefficient of the qPCR reaction mix. Figure 2d shows the thermal cycling of the qPCR mix produced by controlling the laser current. Due to the small nanoliter volume in the cavity and the fast laser-based thermal cycling system, the liquid can be heated/cooled to a specified temperature in a few hundred milliseconds (mean heating rate was approximately 0.1ºC/ms). Meanwhile, the system also has the advantages of real-time temperature feedback, good stability and repeatability.

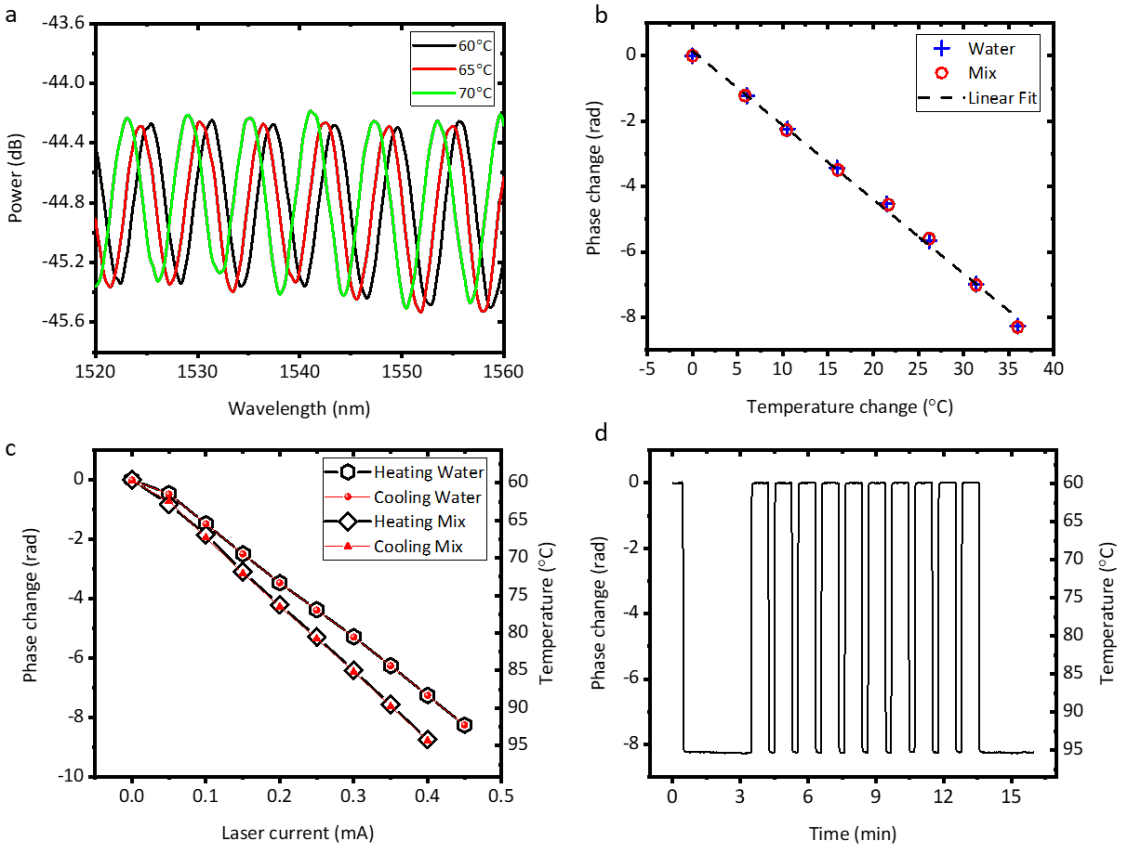

Figure 2. (a) Fabry-Perot interference spectra of the water-filled microcavity at different ambient temperature. (b) Phase change of the Fabry-Perot interference spectra (water and qPCR mix filed microcavity) at different ambient temperatures. (c) Phase change of the Fabry-Perot interference (water and qPCR mix microcavity) spectra with different laser current. (d) Phase change and corresponding temperature of the Fabry-Perot interference spectra (qPCR mix microcavity) with laser current cycling.

3.2 All-fiber all-optical qPCR

Figure 3a and 3b show the fluorescence spectra over 40 qPCR cycles for the NTC and target samples, respectively. It can be seen from Figure 3a that in the absence of target DNA, the change in the fluorescence intensity was negligible with increasing cycles, as expected for a negative control sample. Figure 3b shows that in the reaction containing ACTB gene target DNA (1 ng target DNA per 20 µL reaction volume), the fluorescence intensity increases as a function of the number of cycles, as expected in the qPCR reaction. Figure 3c shows the amplification curves for duplicate NTC and target experiments (separately prepared cavities for each measurement) using our all-fiber qPCR system, which clearly illustrates that the target DNA had been amplified and detected.

We note that there are differences in the amplification curves for the two positive experiments in Figure 3c. The lengths of the cavities are nominally the same (approx. 150 µm), thus the

differences are likely attributed to variations in the sample volume that entered the cavities or errors associated with the sample preparation. Alternatively, there may be subtle differences in the fabrication of the optical fiber system that impacts the excitation and collection efficiency of the fluorescence. In any case, the device shows a clear differentiation between the target and control samples demonstrating that the PCR reaction was carried out as expected.

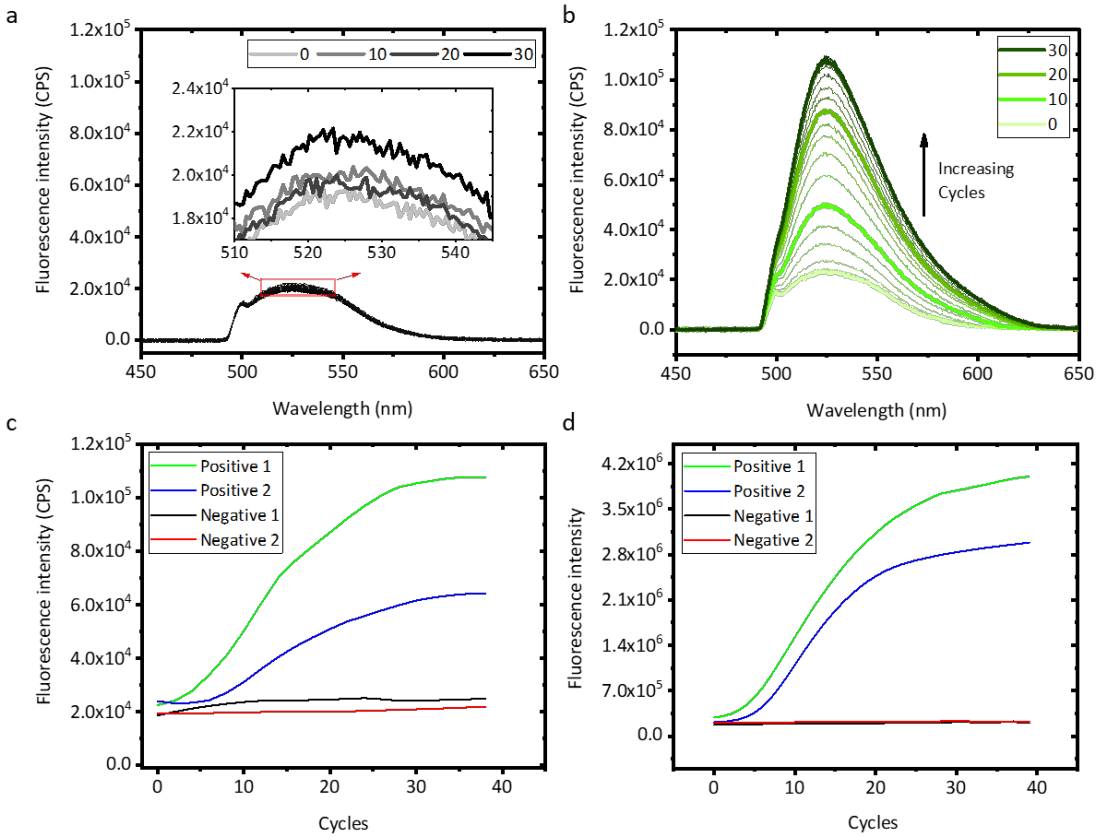

Figure 3. Fluorescence spectra and amplification curves for increasing qPCR cycles. (a) NTC, (b) target, (c) amplification curve from the all-fiber qPCR system, and (d) amplification curve from the ViiaTM 7 Real-Time PCR system. (c), (d) "1" and "2" are replicates.

To verify the amplification results of our all-fiber qPCR system, similar qPCR experiments with the same amplification conditions were conducted using a commercial qPCR system (Viia^{TM} 7 Real-Time PCR system). Figure 3d shows that the amplification curves with two negative and positive experiments run with the Viia^{TM} 7 Real-Time system were consistent with those obtained with our all-fiber system.

Comparing our all-fiber all-optical qPCR system with the commercial qPCR system, the reaction volume was significantly smaller at 0.2 nL compared to 20 µL while the thermal response time was only 450 ms compared to 30 s. This allowed the total reaction to be

completed in only 40 minutes compared to 90 minutes, which could be further optimized by reducing the denaturation and extension times.

3.3 Label-free qPCR

A recent study by Yasui *et al.* demonstrated that DNA amplification can potentially be detected through changes in refractive index of the sample [53]. This can be exploited in our all-fiber qPCR system due to its ability to continuously measure changes in the optical path length inside the microcavity. As was shown in Figure 2, we utilized the change in optical path length to monitor the internal temperature as feedback for the laser that is driving the temperature cycling. However, it is possible to simultaneously monitor any accumulated change in the optical path length that may arise from the PCR amplification process as a result of chemical changes if they lead to refractive index changes. Figure 4a and 4b show the phase changes during the negative and positive qPCR process. In the negative qPCR process, the phase change at 60°C and 95°C remains stable with increasing thermal cycles, while in the positive qPCR process the phase change at 60°C and 95°C decreases with increasing thermal cycles. Figure 4c shows the phase change with increasing cycles in the two negative and two positive qPCR processes (same experiment as from Figure 3). Thus, the refractive index change of the mix reflects the DNA quantity, confirming the potential of the all-fiber all-optical qPCR system to also operate as a label-free qPCR system.

Closer analysis shows different behavior between the interferometer amplification curve (Figure 4c) and the fluorescence amplification curve (from Figure 3c), as shown in Figure 4d. We see that there is a functional difference, with the interferometer initially responding faster compared to the fluorescence detection. This indicates that the refractive index changes are potentially an indirect, rather than direct, measure of the PCR process as the relationship between the number of DNA and the refractive index change is nonlinear. Ideally the refractive index change would be caused by the increasing DNA number, but it may also be a function of increasing free quencher molecules or the linking of the floating nucleotides. While the exact molecular causes need to be further explored, the device clearly shows potential for label-free operation but may require calibrating the DNA number to the refractive index response for given experimental parameters.

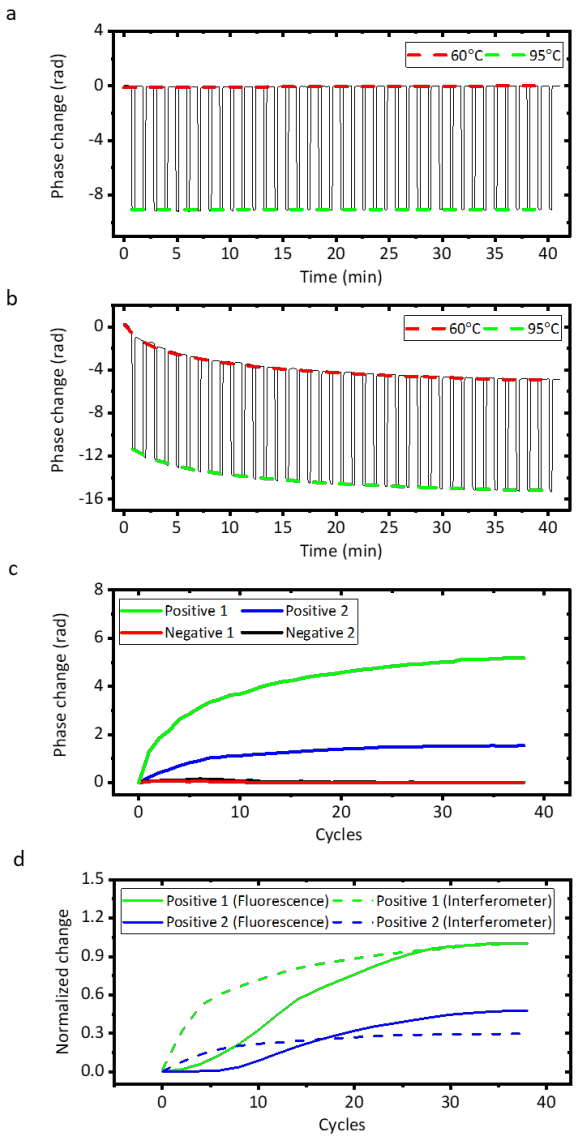

Figure 4. (a) Phase change for increasing qPCR cycles (negative control), (b) phase change for increasing qPCR cycles (target), (c) phase-cycles amplification curve, (d) amplification curve for the fluorescence detection (solid lines) compared to the detection of the Fabry-Perot interferometer phase change (dashed lines). The curves for replicate "1" are normalized to unity for both the interferometer response and the fluorescence response.

4 Discussion

We have demonstrated qPCR using an all-fiber, all-optical system, which offers great opportunity for being implemented as a portable device due to the intrinsic small size of fiber optics. In addition to miniaturizing the back-end optics (lasers and spectrometer), for which there are commercially available solutions, we see the following three keys areas of future development towards the goal of creating field portable qPCR based on fiber optics.

4.1 Multiplexing

For a qPCR system it is important to achieve multichannel amplification. This can be readily achieved in an optical fiber platform, through combination of parallel or in-series configurations. In a parallel configuration, optical couplers and optical switching allows for the use of multiple-channels. Alternatively, the microcavities can be spliced in-series with each cavity having a different length so that the temperature measurement through the Fabry-Perot interference can be demultiplexed. The tradeoff with the parallel configuration is that the infrared heating laser is split between the channels, increasing the requirements for the pump power. Meanwhile, the in-series configuration reduces the flexibility in controlling the infrared laser to achieve the required temperature in each specific cavity. There is also a consideration that the pump, fluorescence, and Fabry-Perot interference signals will degrade as they propagate through each cavity. Therefore, it is likely that multichannel amplification would require the combination of these two configurations.

4.2 Integration with microfluidics for sample preparation

Our all-fiber all-optical qPCR system achieved the amplification of the target DNA with a nanoliter reaction volume. However, the sample was initially prepared with a relatively large volume (20 μL) and only a small fraction was used. This was due to limitations with external pipetting and thus the volume prepared was similar to that used for conventional qPCR equipment. This is a common issue faced by many droplet-based qPCR systems. In future, our platform could be incorporated with microfluidics [54], which has been demonstrated for other optical fiber systems [55]. This could allow for low-volume mixing with higher volumetric precision of the multiple components of the PCR reaction mix to allow for sub-microliter sample usage and device reusability.

4.3 All-optical sample preparation

Kanaka *et* al demonstrated that in addition to driving the thermal cycling of a PCR reaction, an infrared light source could be used in the sample preparation stage such as cell lysis [30]. Our all-fiber all-optical qPCR system also has the possibility of integrating the sample preparation to develop an integrated all-fiber all-optical system for the complete pathway from lysis to qPCR amplification. In addition to improved portability, laser-based cell lysis could offer an effective method for DNA extraction from cells that are difficult to disrupt, such as spores [56].

5. Conclusions

In this paper, we have demonstrated qPCR using an all-fiber, all-optical system with ultra-fast temperature response, real-time temperature feedback, and nanoliter scale reaction volume by using an C-fiber microcavity and ultrafast laser heating system. Further, we demonstrate the potential of the system to operate as a label-free qPCR system through measurement of the

sample refractive index. The method provides the opportunity to implement a fully integrated system, while taking advantage of the optical fiber's well-known characteristics of being small, lightweight, and cheap. We anticipate that this platform technology will offer a new strategy for fundamental techniques in biochemistry applications, such as point-of-care and remote diagnostics, and in-field forensics.

Funding

This work was supported by China Postdoctoral Science Foundation; the National Natural Science Foundation of China under grant [61903073]; Ramsay Fellowship provided by the University of Adelaide; the Optofab node of the Australian National Fabrication Facility utilizing Commonwealth and SA State Government funding; Australian Research Council Centre of Excellence for Nanoscale Biophotonics [CE14010003]; and ARC Linkage project [LP150100657].

Acknowledgments

The authors acknowledge Evan Johnson and Alastair Dowler for their contribution to the fiber fabrication.

Disclosures

The authors declare that there are no conflicts of interest related to this paper.

References

1 Mullis, K., Faloona, F., Scharf, S., Saiki, R., Horn, G. & Erlich, H. Specific enzymatic amplification of DNA in vitro: the polymerase chain reaction. *Cold Spring Harbor Symposia on Quantitative Biology* **51**, 263-273, (1986), doi:10.1101/SQB.1986.051.01.032.

2 Saiki, R., Scharf, S., Faloona, F., Mullis, K., Horn, G., Erlich, H. & Arnheim, N. Enzymatic amplification of beta-globin genomic sequences and restriction site analysis for diagnosis of sickle cell anemia. *Science* **230**, 1350-1354, (1985), doi:10.1126/science.2999980.

3 Williams, R., Peisajovich, S. G., Miller, O. J., Magdassi, S., Tawfik, D. S. & Griffiths, A. D. Amplification of complex gene libraries by emulsion PCR. *Nature Methods* **3**, 545-550, (2006), doi:10.1038/nmeth896.

4 Heckman, K. L. & Pease, L. R. Gene splicing and mutagenesis by PCR-driven overlap extension. *Nature Protocols* **2**, 924-932, (2007), doi:10.1038/nprot.2007.132.

5 Siravegna, G., Marsoni, S., Siena, S. & Bardelli, A. Integrating liquid biopsies into the management of cancer. *Nature Reviews Clinical Oncology* **14**, 531-548, (2017), doi:10.1038/nrclinonc.2017.14.

6 Goodnow, R. A., Dumelin, C. E. & Keefe, A. D. DNA-encoded chemistry: enabling the deeper sampling of chemical space. *Nature Reviews Drug Discovery* **16**, 131-147, (2017), doi:10.1038/nrd.2016.213.

7 Petralia, S. & Conoci, S. PCR Technologies for Point of Care Testing: Progress and Perspectives. *Acs Sensors* **2**, 876-891, (2017), doi:10.1021/acs.sensors.7b00299.

8 Jung, J. Y., Yoon, H. K., An, S., Lee, J. W., Ahn, E.-R., Kim, Y.-J., Park, H.-C., Lee, K., Hwang, J. H. & Lim, S.-K. Rapid oral bacteria detection based on real-time PCR for the forensic identification of saliva. *Scientific Reports* **8**, 10852, (2018), doi:10.1038/s41598-018-29264-2.

9 Castellanos-Rizaldos, E., Grimm, D. G., Tadigotla, V., Hurley, J., Healy, J., Neal, P. L., Sher, M., Venkatesan, R., Karlovich, C., Raponi, M., Krug, A., Noerholm, M., Tannous, J., Tannous, B. A., Raez, L. E. & Skog, J. K. Exosome-Based Detection of EGFR T790M in Plasma from Non-Small Cell Lung Cancer Patients. *Clinical Cancer Research* **24**, 2944-2950, (2018), doi:10.1158/1078-0432.Ccr-17-3369.

10 Choi, W., Yeom, S. Y., Kim, J., Jung, S., Jung, S., Shim, T. S., Kim, S. K., Kang, J. Y., Lee, S. H., Cho, I. J., Choi, J. & Choi, N. Hydrogel micropost-based qPCR for multiplex detection of miRNAs associated with Alzheimer's disease. *Biosensors and Bioelectronics* **101**, 235-244, (2018), doi:10.1016/j.bios.2017.10.039.

11 Tsankov, A. M., Akopian, V., Pop, R., Chetty, S., Gifford, C. A., Daheron, L., Tsankova, N. M. & Meissner, A. A qPCR ScoreCard quantifies the differentiation potential of human pluripotent stem cells. *Nature Biotechnology* **33**, 1182-1192, (2015), doi:10.1038/nbt.3387.

12 Wong, K. H. K., Tessier, S. N., Miyamoto, D. T., Miller, K. L., Bookstaver, L. D., Carey, T. R., Stannard, C. J., Thapar, V., Tai, E. C., Vo, K. D., Emmons, E. S., Pleskow, H. M., Sandlin, R. D., Sequist, L. V., Ting, D. T., Haber, D. A., Maheswaran, S., Stott, S. L. & Toner, M. Whole blood stabilization for the microfluidic isolation and molecular characterization of circulating tumor cells. *Nature Communications* **8**, (2017), doi:10.1038/s41467-017-01705-y.

13 Vera-Rodriguez, M., Chavez, S. L., Rubio, C., Pera, R. A. R. & Simon, C. Prediction model for aneuploidy in early human embryo development revealed by single-cell analysis. *Nature Communications* **6**, 76101, (2015), doi:10.1038/ncomms8601.

14 Spackman, E., Senne, D. A., Myers, T. J., Bulaga, L. L., Garber, L. P., Perdue, M. L., Lohman, K., Daum, L. T. & Suarez, D. L. Development of a Real-Time Reverse Transcriptase PCR assay for type a influenza virus and the avian H5 and H7

hemagglutinin subtypes. *Journal of Clinical Microbiology* **40**, 3256-3260, (2002), doi:10.1128/jcm.40.9.3256-3260.2002.

15 Corman, V. M., Landt, O., Kaiser, M., Molenkamp, R., Meijer, A., Chu, D. K., Bleicker, T., Brünink, S., Schneider, J., Schmidt, M. L., Mulders, D. G., Haagmans, B. L., van der Veer, B., van den Brink, S., Wijsman, L., Goderski, G., Romette, J.-L., Ellis, J., Zambon, M., Peiris, M., Goossens, H., Reusken, C., Koopmans, M. P. & Drosten, C. Detection of 2019 novel coronavirus (2019-nCoV) by real-time RT-PCR. *Eurosurveillance* **25**, 2000045, (2020), doi:10.2807/1560-7917.ES.2020.25.3.2000045.

16 Wang, W., Xu, Y., Gao, R., Lu, R., Han, K., Wu, G. & Tan, W. Detection of SARS-CoV-2 in Different Types of Clinical Specimens. *JAMA*, (2020), doi:10.1001/jama.2020.3786.

17 Mabey, D., Peeling, R. W., Ustianowski, A. & Perkins, M. D. Diagnostics for the developing world. *Nature Reviews Microbiology* **2**, 231-240, (2004), doi:10.1038/nrmicro841.

18 Angus, S. V., Cho, S., Harshman, D. K., Song, J.-Y. & Yoon, J.-Y. A portable, shock-proof, surface-heated droplet PCR system for Escherichia coli detection. *Biosensors and Bioelectronics* **74**, 360-368, (2015), doi:10.1016/j.bios.2015.06.026.

19 Wang, G., Shang, Y., Wang, Y., Tian, H. & Liu, X. Comparison of a loop-mediated isothermal amplification for orf virus withquantitative real-time PCR. *Virology Journal* **10**, 138, (2013), doi:10.1186/1743-422X-10-138.

20 Wu, Z. H., Bai, Y. N., Cheng, Z. L., Liu, F. M., Wang, P., Yang, D. W., Li, G., Jin, Q. H., Mao, H. J. & Zhao, J. L. Absolute quantification of DNA methylation using microfluidic chip-based digital PCR. *Biosensors and Bioelectronics* **96**, 339-344, (2017), doi:10.1016/j.bios.2017.05.021.

21 Chang, Y.-H., Lee, G.-B., Huang, F.-C., Chen, Y.-Y. & Lin, J.-L. Integrated polymerase chain reaction chips utilizing digital microfluidics. *Biomedical Microdevices* **8**, 215-225, (2006), doi:10.1007/s10544-006-8171-y.

22 Ohashi, T., Kuyama, H., Hanafusa, N. & Togawa, Y. A simple device using magnetic transportation for droplet-based PCR. *Biomedical Microdevices* **9**, 695-702, (2007), doi:10.1007/s10544-007-9078-y.

23 Tachibana, H., Saito, M., Shibuya, S., Tsuji, K., Miyagawa, N., Yamanaka, K. & Tamiya, E. On-chip quantitative detection of pathogen genes by autonomous microfluidic PCR platform. *Biosensors and Bioelectronics* **74**, 725-730, (2015), doi:10.1016/j.bios.2015.07.009.

24 Tachibana, H., Saito, M., Shibuya, S., Tsuji, K., Miyagawa, N., Yamanaka, K. & Tamiya, E. On-chip quantitative detection of pathogen genes by autonomous microfluidic PCR platform. *Biosensors & Bioelectronics* **74**, 725-730, (2015), doi:10.1016/j.bios.2015.07.009.

25 Cao, L., Cui, X. Y., Hu, J., Li, Z. D., Choi, J. R., Yang, Q. Z., Lin, M., Ying, H. L. & Xu, F. Advances in digital polymerase chain reaction (dPCR) and its emerging biomedical applications. *Biosensors and Bioelectronics* **90**, 459-474, (2017), doi:10.1016/j.bios.2016.09.082.

26 Baker, M. Digital PCR hits its stride. *Nature Methods* **9**, 541-544, (2012), doi:10.1038/nmeth.2027.

27 Gou, T., Hu, J., Wu, W., Ding, X., Zhou, S., Fang, W. & Mu, Y. Smartphone-based mobile digital PCR device for DNA quantitative analysis with high accuracy. *Biosensors and Bioelectronics* **120**, 144-152, (2018), doi:10.1016/j.bios.2018.08.030.

28 Son, J. H., Cho, B., Hong, S., Lee, S. H., Hoxha, O., Haack, A. J. & Lee, L. P. Ultrafast photonic PCR. *Light-Science & Applications* **4**, 7, (2015), doi:10.1038/lsa.2015.53.

29 Roche, P. J. R., Najih, M., Lee, S. S., Beitel, L. K., Carnevale, M. L., Paliouras, M., Kirk, A. G. & Trifiro, M. A. Real time plasmonic qPCR: how fast is ultra-fast? 30 cycles in 54 seconds. *Analyst* **142**, 1746-1755, (2017), doi:10.1039/c7an00304h.

30 Hettiarachchi, K., Kim, H. & Faris, G. W. Optical manipulation and control of real-time PCR in cell encapsulating microdroplets by IR laser. *Microfluidics and Nanofluidics* **13**, 967-975, (2012), doi:10.1007/s10404-012-1016-5.

31 Kim, H., Dixit, S., Green, C. J. & Faris, G. W. Nanodroplet real-time PCR system with laser assisted heating. *Optics Express* **17**, 218-227, (2009), doi:10.1364/oe.17.000218.

32 Lee, B. Review of the present status of optical fiber sensors. *Optical Fiber Technology* **9**, 57-79, (2003), doi:10.1016/S1068-5200(02)00527-8.

33 Culshaw, B. Optical fiber sensor technologies: opportunities and-perhaps-pitfalls. *Journal of Lightwave Technology* **22**, 39-50, (2004), doi:10.1109/JLT.2003.822139.

34 Choi, S.-J., Yu, H., Jang, J.-S., Kim, M.-H., Kim, S.-J., Jeong, H. S. & Kim, I.-D. Nitrogen-doped single graphene fiber with platinum water dissociation catalyst for wearable humidity sensor. *Small* **14**, 1703934, (2018), doi:10.1002/smll.201703934.

35 Arjmand, M., Saghafifar, H., Alijanianzadeh, M. & Soltanolkotabi, M. A sensitive tapered-fiber optic biosensor for the label-free detection of organophosphate pesticides. *Sensors and Actuators B-Chemical* **249**, 523-532, (2017), doi:10.1016/j.snb.2017.04.121.

36 Li, X., Nguyen, L. V., Zhao, Y., Ebendorff-Heidepriem, H. & Warren-Smith, S. C. High-sensitivity Sagnac-interferometer biosensor based on exposed core microstructured optical fiber. *Sensors and Actuators B-Chemical* **269**, 103-109, (2018), doi:10.1016/j.snb.2018.04.165.

37 Wang, Q. & Wang, B.-T. Surface plasmon resonance biosensor based on graphene oxide/silver coated polymer cladding silica fiber. *Sensors and Actuators B-Chemical* **275**, 332-338, (2018), doi:10.1016/j.snb.2018.08.065.

38 Kim, H.-M., Uh, M., Jeong, D. H., Lee, H.-Y., Park, J.-H. & Lee, S.-K. Localized surface plasmon resonance biosensor using nanopatterned gold particles on the surface of an optical fiber. *Sensors and Actuators B-Chemical* **280**, 183-191, (2019), doi:10.1016/j.snb.2018.10.059.

39 Liu, T., Wang, W., Jian, D., Li, J., Ding, H., Yi, D., Liu, F. & Wang, S. Quantitative remote and on-site Hg2+ detection using the handheld smartphone based optical fiber fluorescence sensor (SOFFS). *Sensors and Actuators B-Chemical* **301**, (2019), doi:10.1016/j.snb.2019.127168.

40 Long, F., Wu, S., He, M., Tong, T. & Shi, H. Ultrasensitive quantum dots-based DNA detection and hybridization kinetics analysis with evanescent wave biosensing platform. *Biosensors & Bioelectronics* **26**, 2390-2395, (2011), doi: 10.1016/j.bios.2010.10.018.

41 Leung, A., Shankar, P. M. & Mutharasan, R. Label-free detection of DNA hybridization using gold-coated tapered fiber optic biosensors (TFOBS) in a flow cell at 1310 nm and 1550 nm. *Sensors and Actuators B: Chemical* **131**, 640-645, (2008), doi:10.1016/j.snb.2007.12.058.

42 Nguyen, L. V., Giannetti, S., Warren-Smith, S. C., Cooper, A., Selleri, S., Cucinotta, A. & Monro, T. M. Genotyping single nucleotide polymorphisms using different molecular beacon multiplexed within a suspended core optical fiber. *Sensors*, 14488-14499, (2014), doi:10.3390/s140814488.

43 Nguyen, L. V., Warren-Smith, S. C., Cooper, A. & Monro, T. M. Molecular beacons immobilized within suspended core optical fiber for specific DNA detection. *Optics Express* **20**, 29378-29385, (2012), doi:10.1364/OE.20.029378.

44 Nguyen, L. V., Hill, K., Warren-Smith, S. & Monro, T. Interferometric-type optical biosensor based on exposed core microstructured optical fiber. *Sensors and Actuators B-Chemical* **221**, 320-327, (2015), doi:10.1016/j.snb.2015.06.068.

45 Xie, L. S., Nguyen, L. V., Ebendorff-Heidepriem, H. & Warren-Smith, S. C. Multiplexed optical fiber biochemical sensing using cascaded C-shaped Fabry-Perot

interferometers. *Ieee Sensors Journal* **19**, 10425-10431, (2019), doi:10.1109/Jsen.2019.2931940.

46 Li, X., Nguyen, L. V., Becker, M., Pham, D., Ebendorff-Heidepriem, H. & Warren-Smith, S. C. Simultaneous measurement of temperature and refractive index using an exposed core microstructured optical fiber. *IEEE Journal of Selected Topics in Quantum Electronics* **26**, 5600107, (2019), doi:10.1109/JSTQE.2019.2908557.

47 Li, X., Warren-Smith, S. C., Ebendorff-Heidepriem, H., Zhang, Y. & Nguyen, L. V. Optical fiber refractive index sensor with low detection limit and large dynamic range using a hybrid fiber interferometer. *Journal of Lightwave Technology* **37**, 2954-2962, (2019), doi:10.1109/JLT.2019.2908023.

48 Warren-Smith, S. C., Kostecki, R., Nguyen, L. V. & Monro, T. M. Fabrication, splicing, Bragg grating writing, and polyelectrolyte functionalization of exposed-core microstructured optical fibers. *Optics Express* **22**, 29493-29504, (2014), doi:10.1364/Oe.22.029493.

49 Curcio, J. A. & Petty, C. C. The near infrared absorption spectrum of liquid water. *Journal of Physical Chemistry A* **41**, 302-304, (1951), doi:10.1021/jp010093m.

50 Kozera, B. & Rapacz, M. Reference genes in real-time PCR. *Journal of Applied Genetics* **54**, 391-406, (2013), doi:10.1007/s13353-013-0173-x.

51 Wu, C., Liu, Z., Zhang, A. P., Guan, B.-O. & Tam, H.-Y. In-line open-cavity Fabry–Pérot interferometer formed by C-shaped fiber fortemperature-insensitive refractive index sensing. *Optics Express* **22**, 21757-21766, (2014), doi:10.1364/OE.22.021757.

52 Ravisankar, M., Reghunath, A., Sathianandan, K. & Nampoori, V. Effect of dissolved NaCl, $MgCl_2$, and Na_2SO_4 in seawater on the optical attenuation in the region from 430 to 630 nm. *Applied optics* **27**, 3887-3894, (1988), doi:10.1364/AO.27.003887.

53 Yasui, T., Ogawa, K., Kaji, N., Nilsson, M., Ajiri, T., Tokeshi, M., Horiike, Y. & Baba, Y. Label-free detection of real-time DNA amplification using a nanofluidic diffraction grating. *Scientific Reports* **6**, 31642, (2016), doi:10.1038/srep31642.

54 Xu, H., Yu, S. Z., Santiago, G. T., Alvarez, M. M., Ribas, J., Jonas, S. J., Weiss, P. S., Andrews, A. M., Aizenberg, J. & Khademhosseini, A. Interplay between materials and microfluidics. *Nature Reviews Materials* **2**, 17016, (2017), doi:10.1038/natrevmats.2017.16.

55 Blue, R. & Uttamchandani, D. Recent advances in optical fiber devices for microfluidics integration. *Journal of Biophotonics* **9**, 13-25, (2016), doi:10.1002/jbio.201500170.

56 Hofmann, O., Murray, K., Wilkinson, A. S., Cox, T. & Manz, A. Laser induced disruption of bacterial spores on a microchip. *Lab on A Chip* **5**, 374-377, (2005), doi:10.1039/b418663j